JOURNAL OF MATERIALS SCIENCE 16 (1981) 1–9

Dark field imaging of semicrystalline polymers by scanning transmission electron microscopy

EDWARD S. SHERMAN, W. WADE ADAMS,* EDWIN L. THOMAS
Polymer Science and Engineering Department, Materials Research Laboratory, University of Massachusetts, Amherst, Massachusetts 01003, USA

Scanning transmission electron microscopy (STEM) has been suggested to have advantages over conventional transmission electron microscopy (CTEM) for the observation of diffraction contrast features and diffraction patterns from radiation sensitive crystalline polymers. Because of image intensification, control of illumination location and magnification independent focus, STEM operation for focusing, area selection and set up of optics permits a high yield of systematic data. Dark field (DF) imaging is most useful when employed in conjunction with scanning microarea diffraction. For convergent beam microdiffraction and efficient DF imaging of thin crystals the beam divergence should be less than 5×10^{-3} radians. For single beam DF, the reflection of interest is selected by the intermediate lens aperture. Use of a STEM annular detector to collect more than one reflection results in increased DF image intensity and resolution. Use of the entire azimuthal range of a single powder pattern reflection permits examination of crystal texture – in particular, images produced by chain axis reflections show the detailed arrangements of lamellae.

1. Introduction

Conventional transmission electron microscopy (CTEM) has become an important technique in studying the microstructure of semicrystalline polymers. Since scanning transmission electron microscopy (STEM) became commercially available a few years ago, more detailed information on polymer morphology is possible using the different imaging techniques of STEM. Recently, we and another group demonstrated the application of STEM in obtaining adjacent microdiffraction patterns from polymers [1, 2].

The purpose of this paper is to explain how STEM can be successfully employed in studying semicrystalline radiation sensitive polymers, particularly with respect to dark field (DF) imaging. The specifics of these techniques pertain to the nondedicated STEM, i.e. a CTEM with a scanning attachment.

2. Operation of STEM for radiation sensitive polymers

Fig. 1 shows schematically the basic components of a STEM. The central feature is a highly focused beam of small diameter (10 to 60 Å for CTEM with a scanning attachment and as low as 2 Å for dedicated STEM) which is sequentially scanned over the thin specimen. The beam is focused onto the specimen by the strong prefield of the objective lens and the transmitted electrons are detected by a photomultiplier tube (PMT). In order to form the image, the amplified signal is displayed on a cathode ray tube (CRT) which is synchronized with the scan coil of the incident illumination. Image contrast arises from variations of the transmitted intensity. The magnification is set by the ratio of the area of the scan on the CRT to the area of the scan on the specimen. The bright field (BF) image is recorded by an on-axis disc

*Present address: Air Force Materials Laboratory, WPAFB, OH 45433.

0022–2461/81/010001–09$02.90/0 © *1981 Chapman and Hall Ltd.*

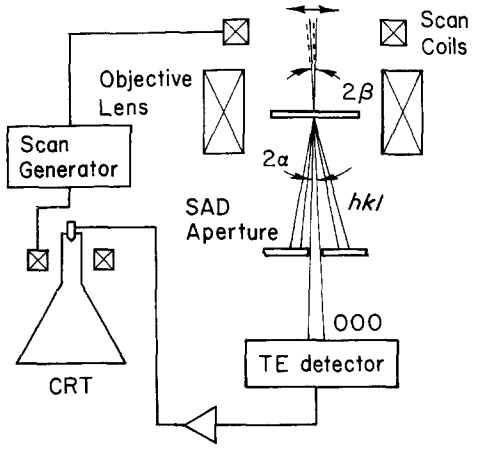

Figure 1 Schematic illustration of the basic components of a STEM.

detector. A second annular detector outside the BF disc detector may be used with a second viewing CRT to provide simultaneous BF and DF images (see Fig. 2). Also, the BF disc detector may be made effectively into an annular detector by blocking out the main transmitted beam with, for example, the diffraction beam stop. For crystalline specimens where a specific reflection is desired to form the DF image, the intermediate lens aperture (SAD aperture) can be used to block out all scattered intensity but the reflection of interest. Because the illumination in STEM is conical, the BF disc detector angle α should be equal to the illumination angle β (see Fig. 1).

STEM has been suggested to have an advantage over CTEM for two principal reasons: (1) the collection efficiency of scattered electrons is higher for STEM than for CTEM and (2) microarea diffraction patterns may be obtained without cumulative radiation damage to adjacent areas [3–5]. Specific comparison between STEM and CTEM depends precisely on the type of incident illumination, mode of image formation, type of image contrast and image resolution desired. Because the STEM image is collected point by point, the various kinds of transmitted electron signals can be processed in many possible ways permitting, for example, selected energy loss images for chemical mapping, elastic to inelastic scattering ratio images for atomic number contrast, etc. [6, 7]. Our approach in this paper will be restricted to applications of STEM DF imaging of radiation sensitive crystalline polymers.

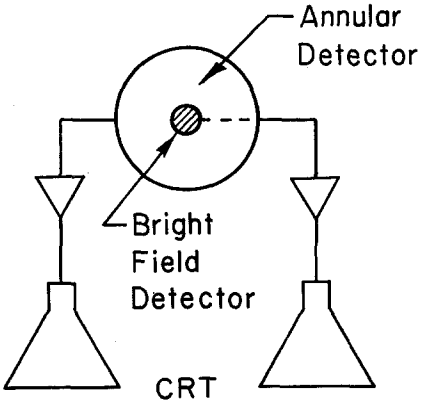

Figure 2 Concentric bright field and annular dark field detector using two amplification and display systems. The bright and dark field images can be observed and recorded simultaneously.

Since radiation damage is the limiting factor in electron microscopy of polymers, the main issue is to consider how to minimize the specimen damage to obtain a given amount of information from the specimen [8, 9]. The electron dose (ϕ_{max}) that can be used to extract information before the sample is severely damaged (thereby making further information more noise than signal) depends only on the radiation physics and chemistry taking place in the sample [8]. This maximum level of damage which can be tolerated depends on what type of information is desired from the specimen. Diffraction contrast images and electron diffraction patterns depend on the crystallinity of the specimen. Because the long range crystalline order of the sample is destroyed with increasing electron dose, a limited number of scattered electrons can be used to obtain crystallographic information. By employing higher accelerating voltages [10] or by specimen cooling, ϕ_{max} may be increased [11]. High voltage does not result in any net improvement because although ϕ_{max} increases, the diffracted intensity per unit incident dose decreases by the same amount. Specimen cooling to cryotemperatures (~ 20 K) results in an approximate 3 x improvement of ϕ_{max} over room temperature for polymers which damage by crosslinking by reducing the mobility and hence the reactivity of the radicals which lead to crosslinking [11]. In addition to improving ϕ_{max}, specimen cooling also increases the scattering efficiency by decreasing the loss of diffracted peak intensity due to thermal diffuse scattering (about 10% increase for polyethylene) [12].

The image resolution, δ, is related to ϕ_{max} by

the equation

$$\delta = \frac{\mathrm{SNR}}{C\left[f\frac{\phi_{\max}}{q}\right]^{1/2}} \quad (1)$$

where SNR is the signal to noise ratio sufficient to detect a signal in a noisy background (it is usually taken as at least 5 [13]), f is the utilization efficiency (i.e. the fraction of the electrons passing through the specimen which contribute to the image), q is the charge of an electron, and C is the contrast [14]. Both f and C are imaging mode dependent. Because f and C are coupled as $f^{1/2}C$, the most efficient use of the transmitted electrons (BF) does not necessarily provide the highest resolution [8, 9].

The only way of improving resolution at a given specimen temperature is thus to increase f [3]. A STEM equipped with an annular detector can collect nearly all electrons scattered outside of the central beam. Optimum information extraction is achieved if all this signal is transferred without loss to the recording medium and if the information loss in the focusing/area selection/diffraction optics set up steps is negligible in comparison to the radiation damage which occurs during recording. The inherent image intensification, control of illumination location and magnification independent focus capabilities of STEM permit a very convenient and precise focusing/area selection/diffraction optics set up without significant radiation damage to the area of interest.

Image intensification is provided by the electronic contrast and brightness controls of the STEM detection system. The electronically manipulated image does not of course contain more information but is merely brighter than the unintensified image [9]. The lower limit at which an ideal image intensification system can be used for focusing or area selection is limited by the statistical electron beam noise to about 1×10^{-14} Amp cm^{-2}. This is a factor of 100 to 200 lower than the necessary current density required for minimum microscope phosphor screen brightness for unaided focusing/area selection by the dark adapted eye [15], provided image intensification does not introduce additional noise (commercial systems approach this ideal [16]). Only the specimen region viewed on the CRT is radiation damaged so that the selected area mode (a variable size reduced raster of the CRT) and variable beam scan speeds are quite useful as discussed in the following example. The specimen is first observed with a rapid scan at low magnification (hence low dose rate). A coarse focus and area selection are accomplished with only slight sample damage. A low quality BF micrograph of the area is taken for reference using the polaroid camera. At this point the selected area mode is used to observe an area from the first selected region that does not contain the precise feature of interest but is sufficiently close so that focusing on this second region will give adequate focus for the desired area. Since focus is independent of magnification in STEM (which is not the case for CTEM) the image is focused for high resolution at a high magnification in the selected area mode with a slow scan speed to improve SNR for precise focus, damaging (severely) only a very small area. The magnification is then reduced and a full CRT scan is used to record a high resolution image from a nearby undamaged, in focus, selected area. Fig. 3 is a BF micrograph taken of a polyethylene single crystal using this method. (Note the nondiffracting area which was damaged during selected area focusing.)

3. STEM dark field of crystalline polymers

Inherent to all DF imaging is proper selection of the portion of the diffraction pattern which will be used to form the DF image. Such selection is possible by employing relatively low incident beam divergence so that discrete diffraction spots can be resolved in the diffraction pattern. This condition is commonly called convergent beam diffraction [17]. For our JEOL 100 CX microscope, a small (~ 20 μm diameter) second condenser

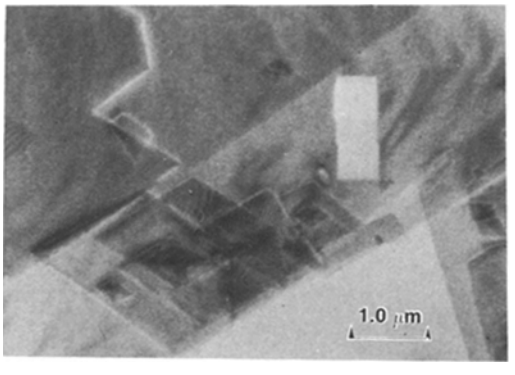

Figure 3 Bright field micrograph of overgrown polyethylene single crystals. The rectangular region in the upper right is lighter and lacks contrast because it was radiation damaged during focusing at high magnification.

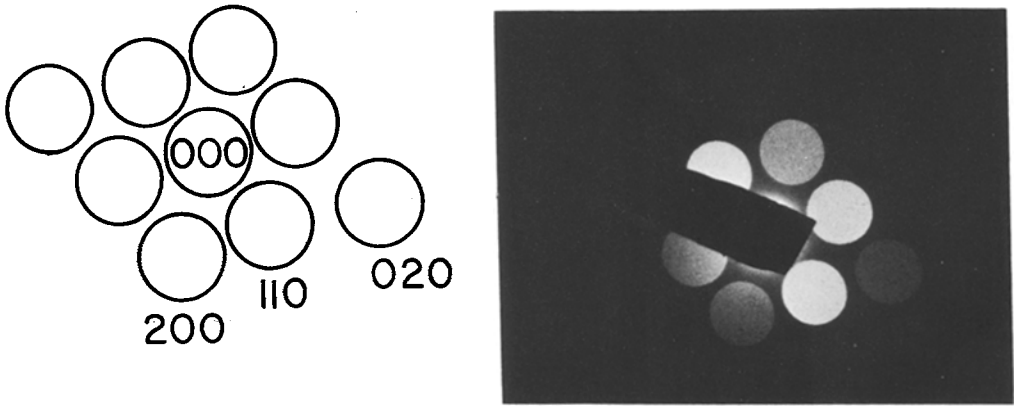

Figure 4 STEM microarea diffraction pattern from a polyethylene single crystal with beam stop tip for annular DF in position. The reflections are broad due to the large divergence of the incident beam.

aperture with a 60 Å electron probe diameter permits the individual reflections of a polyethylene single crystal to be resolved (see Fig. 4). For these conditions, the contribution of beam size to the line width of the reflections is small in comparison to that from beam divergence [1]. The minimum polymer sample size which can form a useful diffraction pattern is limited by the insufficient signal to noise statistics in the scattered peaks at low doses and by destruction of the crystal by radiation damage at high doses. By *scanning* the beam and systematically varying the size of the scanned area at fixed incident beam current, the smallest area (for a given sample thickness) which yields a "useful" scanning microarea diffraction pattern can be determined. Successive adjacent area scanning microarea diffraction patterns for mapping the specimen crystallography in the region of interest can be obtained routinely since the selected area scan mode can be adjusted to the desired size, shape and location on the sample with the incident beam off [1].

There are several methods of obtaining STEM DF images. If all but one of the reflections are restricted (by the SAD aperture) from reaching the PMT detector, the conventional single beam DF image is obtained. Various types of multiple beam DF images are possible with STEM. In principle, such images could be obtained in CTEM, i.e. using the strioscopy technique where the main beam is blocked by a fine wire placed across the objective aperture, or by using hollow cone illumination. Besides being a very exacting technique, multiple beam CTEM DF imaging is resolution limited by spherical aberration and objective lens defocus image displacements [18]. Because STEM imaging is not so affected, the annular DF detector may be usefully employed to increase the utilization efficiency of the scattered signal. Although beam divergence is not normally important for CTEM DF imaging the rather large beam divergences encountered in STEM imaging must be considered.

Beam divergence and beam diameter are inversely related. The beam divergence β (defined as half the total angular width of the incident beam) can typically vary from about 1×10^{-3} radians for a 200 Å diameter beam (microdiffraction mode) to about 5×10^{-2} radians for a 10 Å beam (high resolution imaging mode). The effect of increased beam divergence will be to decrease the diffracted intensity and to broaden the reflections. The DF image efficiency will of course depend on the diffracted intensity. The diffracted intensity is governed by the well known equation for the rocking curve.

$$I(s) \sim |F(h\,k\,l)|^2 \frac{\sin^2 \pi s t}{\sin^2 \pi s} \qquad (2)$$

where $F(h\,k\,l)$ is the structure factor for the $(h\,k\,l)$ reflection, t is the crystal thickness parallel to the optic axis and s is the deviation of the $(h\,k\,l)$ planes to be imaged from the Bragg condition ($s = 0$). The magnitude of s depends on the magnitude of the diffraction vector of the reflection used, g, and the amount of divergence of the beam ($s \simeq g\beta$). Since the STEM illumination is conical, there is a distribution of s. If, as is usual, the second condenser aperture is evenly illuminated, this incident intensity distribution $\rho(\beta)$ will be

$$\rho(\beta) = \begin{matrix} 1 \text{ if } |\beta| < \beta^* \\ 0 \text{ if } |\beta| \geqslant \beta^*. \end{matrix} \qquad (3)$$

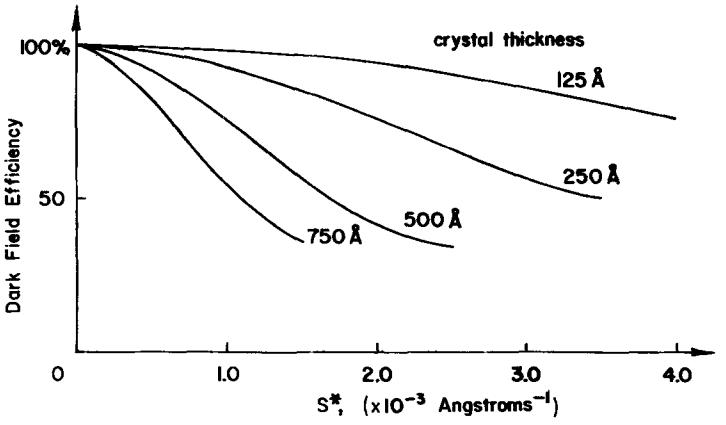

Figure 5 Dark field efficiency for various crystal thicknesses as a function of the maximum deviation parameter.

Thus the scattered intensity of a reflection g with an incident beam divergence of β^* will be given by

$$I_g(s^*) \simeq |F_g|^2 \int_{-g\beta^*}^{g\beta^*} \rho(s) \frac{\sin^2 \pi s t}{\sin^2 \pi s} \mathrm{d}s. \qquad (4)$$

For a perfectly parallel incident beam ($\beta^* = 0$), the scattered intensity will be proportional to t^2. Fig. 5 shows calculated curves of the scattering efficiency (defined as $I(s^*)/t^2$) as a function of the maximum deviation parameter s^* for different crystal thicknesses. For the typical beam divergence range ($1 \times 10^{-3} < \beta < 5 \times 10^{-2}$ radians) the maximum deviation parameter varies from approximately 0.2 to 1.0×10^{-3} Å^{-1}. It is apparent that for thick crystals a significant portion of the possible Bragg scattered intensity could be lost. The beam divergence thus should be kept below about 5×10^{-3} radians. This requires about a 20 μm diameter second condenser aperture (instead of the normal 100 μm) to yield a low divergence small diameter beam (although now of relatively low brightness – requiring increased gun brightness and decreased beam scan rates).

A large divergence can also be useful. For a very parallel illuminating beam, as in CTEM, Bragg diffraction is strong for only a limited tilt range of the crystal. STEM will image crystals in DF over a greater tilt range than CTEM, however, the images of the crystals will be somewhat less intense because of the larger beam divergence. On average more crystals will be imaged per unit area and the image will be less sensitive to tilt of the crystallites. It should be mentioned that when several diffracted beams contribute to the image, diffraction contrast image interpretation is rather complicated. The least efficient, tilted CTEM single beam dark field mode provides the easiest interpretation since both the diffraction vector g and the deviation parameter s are unique.

4. Applications

We have employed the multiple reflection (n beam) DF technique in several ways. By simply blocking the main beam with the diffraction beam stop tip a DF image employing all excited reflections is produced. This type of DF image is essentially the complement of the BF image. Depending on the orientation, it is possible for several reflections from the same crystal to contribute to that crystal's image, resulting in a higher SNR than for a single beam DF. The image intensity of a crystal will be proportional to the crystal thickness along the optic axis, the number of reflections contributing and their respective structure factors. The resolution improvement attainable depends on the square root of the intensity enhancement. For a polyethylene crystal with the ($h\,k\,0$) reciprocal lattice orientation (a rather favourable situation for n beam imaging) the n beam image (n is about 20 beams) by structure factor calculation (room temperature 100 kV) should be approximately 9 x more intense [19]. This would result in a 3 x improvement in resolution. Since single beam g_{110} DF resolution is estimated at about 40 Å for a 120 Å thick lamella [8, 9], STEM annular n beam DF for this crystal orientation should yield a resolution of perhaps 15 Å – the same as the practical beam size limited resolution of a tungsten hairpin filament STEM.

An example of the intensity enhancement of an n beam annular DF image compared with a single beam DF image for a polyethylene single crystal is shown in Fig. 6. By using the selected area mode for microdiffraction the optics were

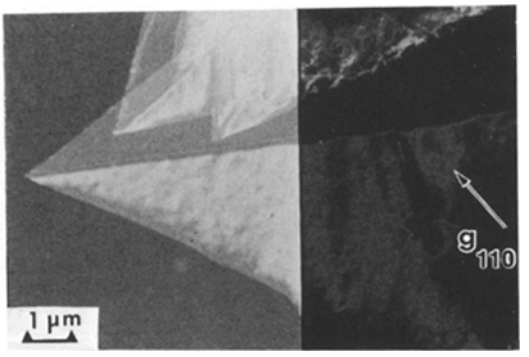

Figure 6 STEM *n* beam annular versus single beam dark field for two halves of the same single crystal. Spot size approximately 60 Å, beam divergence 3.7×10^{-3} radians.

adjusted so that the left half of the crystal was imaged by the annular DF mode and the right half was imaged using single beam g_{110} DF. Images of both halves were recorded under identical illumination conditions.

In order to demonstrate improved image resolution by STEM DF, some reliably known convenient scale (15 to 100 Å) high diffraction contrast objects must be present. The crystallite blocks in microfibrils represent such objects. Fig. 7a is a STEM annular DF image of microfibrils within a microneck zone of a deformed spherulitic polyethylene film. The relatively undeformed regions on either side of the transformation zone are overexposed in this micrograph because of the greater sample thickness. Small 50 to 200 Å diameter crystallites alternate along the fibril axis with thin nondiffracting regions. In the enlargement (Fig. 7b) the crystallites appear with rounded corners because of the approximately 15 Å incident beam diameter. Arrows point to adjacent diffracting crystallites separated by 25 Å.

A systematic STEM DF study of an oriented polyethylene film is shown in Fig. 8a to c. These micrographs were taken at 10 000 × magnification and are part of a tilt series which includes 6 STEM DF images and 2 CTEM BF images. The 4 circular nondiffracting areas are from the regions used to obtain microdiffraction patterns. The tilt axis is shown in Fig. 8a. Arrows point to selected lamellae which change their image intensity with angle of tilt.

Annular *n* beam DF imaging is also very useful for detecting various types of crystalline material present only in a small volume fraction of the sample. Normally reflections from such a low volume fraction species would be totally obscured in the diffraction pattern, making it nearly impossible to locate properly (only by trial and error) the reflections of interest in the objective aperture. With STEM annular DF however, all regions which diffract are imaged. Fig. 9 shows an example of the DF imaging of intercrystalline links by this method. A sample of polyethylene was co-crystallized with a low-molecular weight paraffin and the paraffin subsequently solvent extracted to reveal the intercrystalline links between adjacent lamellae [20]. The arrows in the figure indicate the intercrystalline links which appear *not* to be continuously crystalline along their length as was previously suggested [20] but appear to be composed of alternating crystalline and noncrystalline regions.

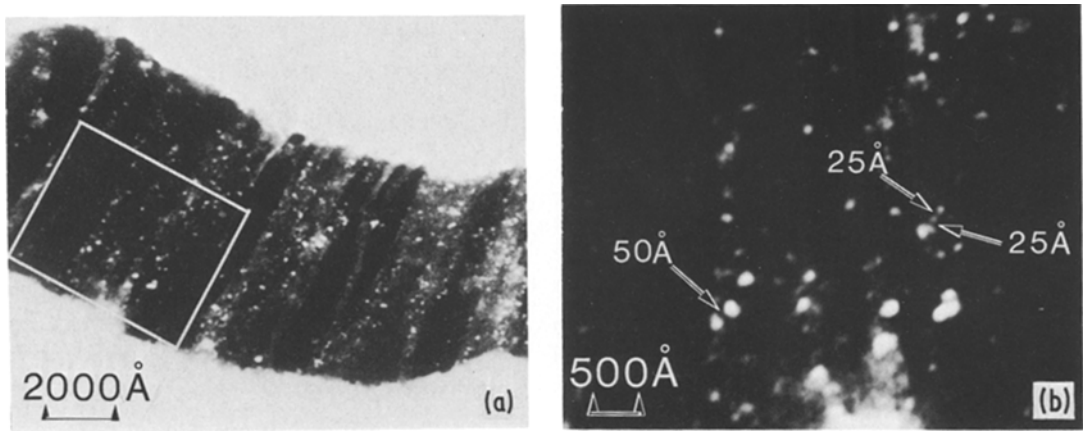

Figure 7 STEM *n* beam annular DF image showing 50 to 200 Å diameter diffracting microfibril crystallites within the microneck zone of a deformed spherulitic polyethylene film.

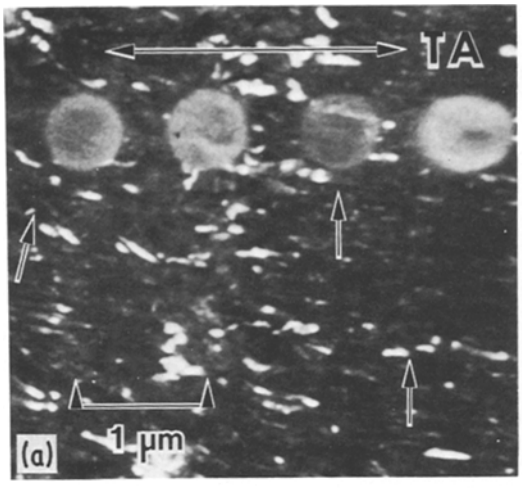

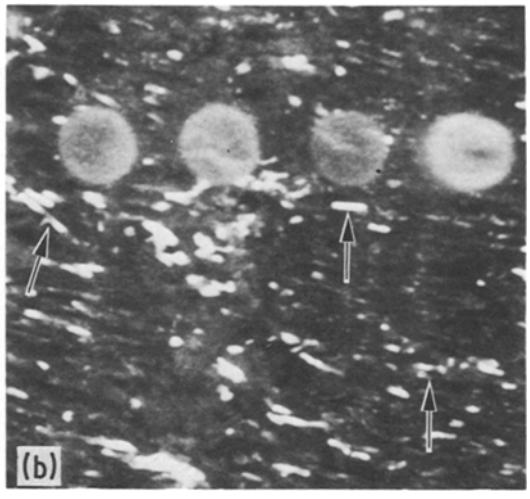

Figure 8 STEM *n* beam annular DF tilt series of oriented polyethylene lamellar film. TA indicates the tilt axis. (a) + 1° tilt (b) 0° tilt and (c) − 2° tilt.

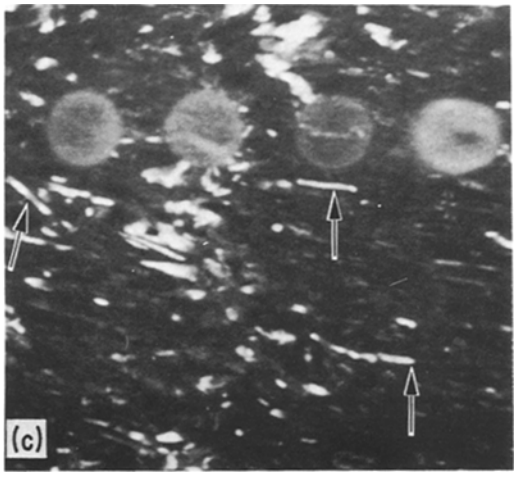

Another annular DF mode is to allow only a single diffraction ring from a sample exhibiting a powder pattern to reach the detector. This may be accomplished by a suitable combination of beam stop size and diffraction pattern size [which may be varied using one of the lenses below the specimen (intermediate lens)]. Such an image will reveal all azimuthal orientations of crystals with the given $(h\,k\,l)$ plane at the Bragg angle. Fig. 10c shows an example of the single powder reflection annual DF image for a spherulitic polyethylene film employing g_{002}. Fig. 10a and b are BF and *n* beam annular DF images of the same area as Fig. 10c. Except for slight changes in orientation of the film between exposures, it is apparent that the *n* beam annular DF image is complementary to the BF image. The single powder reflection annular DF image is much simpler in appearance, making for more straightforward image interpretation as compared to the *n* beam image since the chain axis reflection image shows only the thin lamellar crystals oriented with their chain axis in the plane of the specimen film. This technique is thus very suitable for studying the rotation and orientation of lamellae during deformation. Furthermore, one obtains a direct measure of the crystal thickness along the chain direction, which is useful to compare with that determined by small angle X-ray and laser Raman methods.

5. Conclusions

The typical approach to CTEM DF imaging of radiation sensitive polymers is to focus in bright

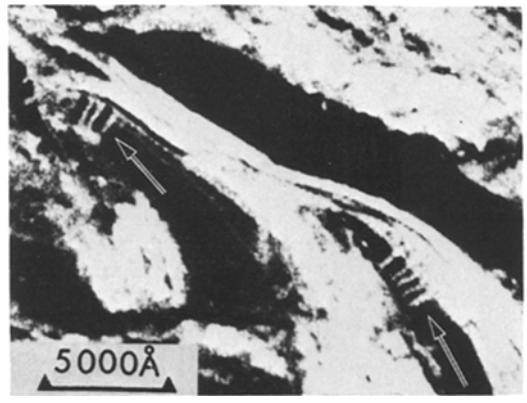

Figure 9 STEM *n* beam annular DF image of intercrystalline bridges in spherulitic polyethylene. Arrows indicate the bridges which consist of alternating crystalline and noncrystalline regions.

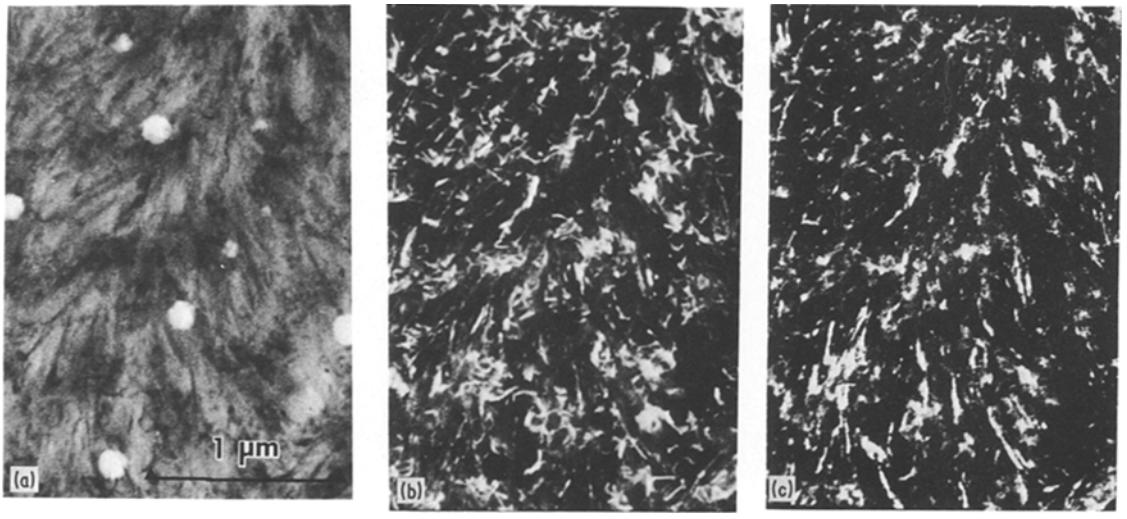

Figure 10 (a) STEM BF image of spherulitic polyethylene films. (b) STEM *n* beam annular DF image of same region as (a). (c) STEM 002 annular DF image of same region as (a).

field, insert the objective aperture in the diffraction pattern, translate to an adjacent undamaged area and record the (single beam) DF image. The disadvantage of this approach is a low yield of useful micrographs due to focusing errors and blind selection of diffraction optics and specimen areas. This method is clearly difficult for performing systematic studies. Because of image intensification, control of illumination location and magnification independent focus, STEM operation for focusing, area selection and optic set up permits a high yield of systematic data.

STEM DF imaging may be done with one or more reflections. For convergent beam microdiffraction and efficient DF imaging of thin crystals, a small second condenser aperture should be employed so that the beam divergence is less than 5×10^{-3} radians. Use of *n* beam annular DF allows investigation of crystalline species present only in small volume fractions. *n* beam annular DF is a high contrast complement to the BF image. Use of the entire azimuthal range of a single powder pattern reflection permits examination of crystal texture – in particular, images produced by chain axis reflections show the detailed arrangements of lamellae. By using more than one reflection to image a crystal, the DF image intensity and resolution are increased. In the most favourable cases, *n* beam DF imaging will yield at most a 3 × improvement in resolution, or for a given resolution, a 9 × increased number of micrographs over single beam DF.

Acknowledgement

This research was carried out with financial support of the National Science Foundation, Grant DMR 77-24955, Polymers Programme.

References

1. E. S. SHERMAN and E. L. THOMAS, *J. Mater. Sci.* **14** (1979) 1109.
2. A. LOW, D. VESLEY, P. ALLEN and M. BEVIS, *ibid.* **13** (1978) 711.
3. J. LANGMORE, J. WALL and M. S. ISSACSON, *Optik* **38** (1973) 335.
4. M. G. R. THOMSON in "Physical Aspects of Electron Microscopy and Analysis", edited by B. M. Siegel and D. R. Beaman (John Wiley, New York, 1975) p. 47.
5. A. ENGEL, J. DUBOUCHET and E. KELLENBERGER, *SEM Proceedings* **1** (1977) 377.
6. J. M. COWLEY and A. Y. AU, *ibid.* **1** (1978) 53.
7. A. ROSE, *Optik* **39** (1979) 416.
8. D. T. GRUBB, *J. Mater. Sci.* **9** (1974) 1715.
9. E. L. THOMAS and D. G. AST, *Polymer* **15** (1974) 37.
10. L. E. THOMAS, D. J. HUMPHREYS, W. R. DUFF and D. T. GRUBB, *Rad. Eff.* **3** (1971) 89.
11. D. T. GRUBB and G. W. GROVES, *Phil. Mag.* **24** (1971) 815.
12. E. L. THOMAS and S. L. SASS, *Die Makro. Chemie* **164** (1973) 333.
13. A. ROSE, *Adv. Electron.* **1** (1948) 131.
14. M. ISSACSON, D. JOHNSON and A. V. CREWE, *Rad. Res.* **55** (1973) 205.
15. A. AGAR, *Brit. J. Appl. Phys.* **8** (1957) 410.
16. K. H. HERMAN, D. KRAHL and V. RINDFLEISH, *Siemens Forsch. Entwickl. Ber.* **1** (1972) 167.
17. W. KOSSEL and G. MOLLENSTADT, *Ann. Physik* **5** (1939) 36.

18. E. L. THOMAS, *J. Mater. Sci.* **12** (1977) 234.
19. *Idem,* in "Developments in Electron Microscopy and Analysis", edited by J. A. Venables (Academic Press, London, 1976) p. 293.
20. H. D. KEITH, F. J. PADDEN and R. G. VADIMSKY, *J. Appl. Phys.* **42** (1971) 4585.

Received 20 February and accepted 5 June 1980.